



HAL
open science

A “wave automaton” for wave propagation in the time domain: II. Random systems

Patrick Sebbah, Didier Sornette, Christian Vanneste

► **To cite this version:**

Patrick Sebbah, Didier Sornette, Christian Vanneste. A “wave automaton” for wave propagation in the time domain: II. Random systems. *Journal de Physique I*, 1993, 3 (6), pp.1281-1302. 10.1051/jp1:1993155 . jpa-00246797

HAL Id: jpa-00246797

<https://hal.science/jpa-00246797>

Submitted on 4 Feb 2008

HAL is a multi-disciplinary open access archive for the deposit and dissemination of scientific research documents, whether they are published or not. The documents may come from teaching and research institutions in France or abroad, or from public or private research centers.

L’archive ouverte pluridisciplinaire **HAL**, est destinée au dépôt et à la diffusion de documents scientifiques de niveau recherche, publiés ou non, émanant des établissements d’enseignement et de recherche français ou étrangers, des laboratoires publics ou privés.

Classification

Physics Abstracts

71.55J — 03.40K — 42.20

A « wave automaton » for wave propagation in the time domain : II. Random systems

Patrick Sebbah, Didier Sornette and Christian Vanneste

Laboratoire de Physique de la Matière Condensée (*), Université de Nice-Sophia Antipolis, Parc Valrose, B.P. 71, 06108 Nice Cedex 2, France

(Received 22 December 1992, revised 9 February 1993, accepted 17 February 1993)

Abstract. — Following our previous description of the « wave automaton », a new lattice model introduced for the *dynamical* propagation of waves in arbitrary heterogeneous media which is efficient for calculations on large systems ($1\,024 \times 1\,024$) over long times (several 10^6 inverse band widths), we present a detailed study of the time-dependent transport of wave packets in 2D-random systems. The scattering of a Bloch wave in a periodic system by a single impurity is first calculated analytically, which allows us to derive the elastic mean free time τ and mean free length ℓ_e as a function of the model parameters and the frequency $f = \omega/2\pi$. We then expose the different results on wave packets in random media which have been obtained using extensive numerical simulations on a parallel computer. We study the different regimes (ballistic, diffusive, localized) which appear as the wave packets spread over the random media and compare these numerical results with weak localization predictions.

1. Introduction.

The wave automaton model, described in detail in the previous paper [1], is a lattice model of wave propagation in arbitrary media. It is probably the simplest model to capture the essentials of wave propagation in discrete lattices. Its construction in real space and time makes it ideally designed for studying time-dependent properties of wave propagation in large arbitrary random media at long times. Although this model is analogous, in some range of parameters, to a time dependent tight-binding model with second-nearest neighbor coupling (as has been shown in [1]), its formulation is however quite different from the usual formulation of tight-binding models. Usually, dealing with wave propagation in heterogeneous media implies the resolution of an equation (eg. Schrödinger equation), using a Hamiltonian H (eg. $H\Psi_i = V_i\Psi_i + J \sum_{|i-j|=1} \Psi_j$ for the tight-binding model). Unfortunately, the time evolution is not given by

(*) CNRS URA 190.

H directly but by its exponentiated form, the evolution operator $U = e^{iH\tau} = 1 - iH\tau - H^2 \tau^2/2 + \dots$. Numerical calculations then usually need a scheme to approximate $e^{iH\tau}$ which may lead either to errors which end up accumulating at long times or to complex numerical operations slowing down the computation significantly. Again, the specificity of our model is that it is the evolution operator U which is postulated from the start. Besides, because the S-matrix is unitary, U is also perfectly unitary. Except for the calculator precision itself, the problem of energy drifting is eliminated and the number of iterations can be drastically increased, enabling computation of the dynamics over very large times (up to several 10^6 time steps with double precision numbers). U processes the scattering and the conversion of the output field into the new input field. A detailed discussion of more standard numerical methods used to integrated time-dependent equations can be found in [2-4].

In the wave automaton, narrow pulses $A e^{i\phi}$ propagate along the bonds of a lattice (for instance square or triangular in 2D, cubic in 3D). The impinging pulses on each node of the lattice are instantaneously and simultaneously scattered by a z by z S-matrix (where z is the coordinate number) in the time domain into outgoing pulses which then propagate in a unit time to the neighboring nodes. Energy conservation and invariance with respect to time-reversal imply that the S-matrices must be unitary and symmetric. For an isotropic square (2D) or cubic (3D) lattice, each S-matrix is parametrized by three complex parameters: t (the transmission amplitude in the direction of the incident wave pulse), r (the amplitude reflected along the incident bond) and d (the amplitude scattered in each channel at $\pi/2$), which obey the following conditions, $|t|^2 + |r|^2 + (z-2)|d|^2 = 1$, and $rt^* + r^*t + (z-2)|d|^2 = 0$ and $(r+t)d^* + (r^*+t^*)d + (z-4)|d|^2 = 0$ (with $z = 4$ in 2D and $z = 6$ in 3D). In our previous notation [1], for the 2D case,

$$t = e^{2i\alpha} [\cos \delta + 1]/2 \quad (1a)$$

$$r = e^{2i\alpha} [\cos \delta - 1]/2 \quad (1b)$$

$$d = (i/2) e^{2i\alpha} \sin \delta \quad (1c)$$

where $0 \leq \delta \leq \pi$ and $0 \leq \alpha \leq \pi$ are real parameters. The parameter δ is a measure of the scattering strength and α is a measure of the phase shift acquired by the wave at each encounter with the scatterer. For $\delta = 0$, the S-matrix is transparent and the wave crosses over the node keeping the same direction while taking a phase shift equal to 2α . This is the 1D-limit since the 2D lattice can be considered as a set of independent horizontal and vertical lines on which waves propagate without distortions. At the other extreme $\delta = \pi$, the reflection coefficient is equal to $-e^{2i\alpha}$ and is of unit modulus whereas all other processes disappear. The node possessing such an S-matrix is perfectly reflecting. Varying δ between 0 and π then allows us to weight the strength of the three scattering processes (transmission, reflection and $\pi/2$ scattering) continuously.

A given system will then be defined by the set of 4 by 4 unitary symmetric S-matrices parametrized using equation (1), with one S-matrix per node, i.e. one couple (δ, α) per node. The case where all the S-matrices are the same on all nodes corresponds to a periodic system, which was studied in detail in our previous paper [1]. A quenched random system is defined by a set of S-matrices, one for each node, with random choices for the real parameters α and δ . We can also choose to take the same δ for all matrices and take random choices for α . The latter model has the advantage that all S-matrices have the same scattering efficiency (same scattering cross sections) and differ only by the phase shift taken by a scattered wave. Thus, the emphasis is put on the wave phase, which turns out to be useful to study Anderson wave localization, a phenomenon deeply associated with phase coherence. This is the choice that has been made in our computations reported below. The parameters of the model for a given random system are the scattering strength δ of the S-matrices and the width

$\Delta\alpha$ in which the random phase α , which is randomly chosen from one node to another : $\alpha \in [-\Delta\alpha ; +\Delta\alpha]$.

A significant advantage of our model is that it can be easily implemented on SIMD parallel architectures (in that, it is of course not unique). In fact, its parallelisation is obvious : each virtual processor of the machine is associated with a scatterer at a node of the square lattice and all scattering processes are performed simultaneously. This allows large 2D system sizes (up to 1 024 by 1 024 on a 32 K Connection Machine) to be used. These are useful to minimize finite size effects and to observe all the different regimes of time propagation with good accuracy. It also makes reasonable the future study of 3D system of sizes of order 128^3 .

The « Wave Automaton » was implemented on the Connection Machine (CM200) of I.N.R.I.A. (Sophia-Antipolis) and the CM2 of the IPG (Paris). A first sequence generates simultaneously the S-matrices, calculated for given values of the scattering strength δ and the disorder parameter $\Delta\alpha$. We recall that in most of our computations the scattering strength δ is the same for all the S-matrices in the lattice when not otherwise specified and the random phase α is randomly and uniformly chosen from one node to another in the interval $\alpha \in [-\Delta\alpha, +\Delta\alpha]$. The set of S-matrices is then stored on the Datavault, the parallel memory of the CM. Note that one could also easily generate a different set of S-matrices at each time step in order to study wave propagation in time dependent disordered systems, such as in turbulent media. This problem is left for future studies.

The second step of the computation is the dynamic sequence. A vector of $2L^2$ components (for waves propagating on only one of the sublattices [1]) is constructed to describe the field entering the four bonds surrounding the $L^2/2$ scatterers. A second vector of $2L^2$ components is also constructed to describe the outgoing field on each node after the scattering process. The parallel computer performs $L^2/2$ matrix-vector products simultaneously. Then, the outgoing vector becomes the new input vector using a simple shift to the next four neighboring scatterers. Since the time consumption of first neighbor communication is negligible on the CM2 architecture, the speed of the program depends only on the time consumption associated with the scattering process (matrix-vector products). The program reaches typically 1 Gigaflops when working on two sequencers (16 K processors) on a CM200. The additional calculations of other physical quantities, such as the radius of gyration of the wave packet, slightly slow it down.

Finally, one has the freedom of the initial conditions, i.e. how the wave energy is injected within the system. We have worked by launching either a field impulse in time and space (i.e. we fix the field at the origin of time and space and then let the wave propagate), thus exciting the whole range of the spectrum, or by launching a wave packet of width $\Delta\omega$ centered around a specific pulsation ω_0 , enabling the study of the dynamical interaction of a few modes which are spatially localized in the neighborhood of the injection site. Computations with such wave packets have permitted a test of weak localization predictions in the time domain [5] (see Sect. 3 below). We have also used a source localized on one site and oscillating at some specific pulsation ω_0 , chosen to be an eigenfrequency of the system (the eigenfrequencies are obtained by Fourier transform of a long time sequence of the field at the origin, in the case where an impulse is launched (see below)). By increasing very slowly the amplitude of the source at ω_0 , one can thus construct the spatial structure of the eigenmode at pulsation ω_0 .

In section 2, we treat the case of the interaction of a Bloch wave with a single impurity (corresponding to a different S-matrix on one node in a « sea » of identical S-matrices). The scattered Bloch wave is calculated analytically which allows us to derive the elastic mean free time τ and mean free length l_e as a function of the model parameters and the frequency $f = \omega/2\pi$. These parameters are used in the next section (Sect. 3) to compare quantitatively

the numerical results of wave propagation in random media with predictions from weak localization theory. In section 3, we describe the different results that have been obtained using extensive numerical simulations of wave packets in random media. We particularly study the different regimes (ballistic, diffusive, localized) which appear as the wave packets spread over the random media and compare these numerical results with weak localization predictions.

2. Weakly disordered systems.

We consider the case of quenched disordered systems, obtained by choosing the phase α independently from node to node and randomly in the interval $[-\Delta\alpha, +\Delta\alpha]$, while still keeping the parameter δ identical in all S-matrices. $\Delta\alpha$ is then a measure of the strength of the disorder : if $\Delta\alpha$ is close to zero, the disorder is weak ; when $\Delta\alpha$ is close to $\pi/2$, the disorder is maximum. In order to analyse the weak disorder limit, it is also useful to consider disordered systems constructed by random dilution, i.e. where randomly chosen nodes at large distances from each other possess a S-matrix with a different phase α' from the rest of the nodes which have all identical S-matrices. This structure gives sense to the limit of well-defined Bloch waves interacting with isolated scatterers. The mean free path ℓ_e (or equivalently the mean free time $\tau_e = \ell_e/c$) which is the key variable to characterize a random system in a general way, then takes the simple meaning of the effective length between efficient interactions between the Bloch modes and the scatterers (note that ℓ_e is in general much larger than the distance between scatterers since a single scatterer is often too weak to scatter significantly the incident Bloch off its propagation direction). At lengths smaller than ℓ_e , the wave is essentially propagating : its energy travels at an average speed c of the wave in the medium and the scatterers have not yet made a significant contribution except for renormalizing the effective velocity [6]. The regime where one considers scales $|r|$ less than ℓ_e , such that $\ell_e \gg \lambda$ the wavelength, is called the weak disorder regime.

A first estimate of the dependence of the mean free path ℓ_e on the parameters δ and $\Delta\alpha$ can be obtained in the limit of small scattering strengths δ , such that the modulus of the transmission coefficient is close to one. In this case, the $\pi/2$ -scattering events are weak (of amplitude of order δ) and the lattice can be considered as a set of horizontal and vertical lines which are weakly coupled transversely. Selecting a direction of propagation along one of the axe, say Ox, the propagation along Ox is then approximately described at scales less than ℓ_e by the tight-binding equation $|t|(\Psi_{n+1} + \Psi_{n-1}) + V_n \Psi_n = 0$, where the hopping coefficient is identified with the modulus $|t| = \cos^2 \delta/2$ of the transmission coefficient and the on-site potential V_n is, according to the Fermi golden rule, proportional to the square root of the scattering cross section $\sigma_e = 1 - \cos^4 \delta/2$ (Eq. (13) [1]). We can then use the 1D expression for the mean free path [7]

$$\ell_e = 4 |t|^2 \sin^2 |\mathbf{k}| / [\langle V_n^2 \rangle - \langle V_n \rangle^2] \quad (2)$$

where $\langle . \rangle$ means an averaging over the disorder in the realizations of α . We estimate the term $\langle V_n^2 \rangle - \langle V_n \rangle^2$ by writing $V_n = V_0 [1 - \cos^4 \delta/2]^{1/2} e^{2i\alpha_n}$, since all the scattering amplitudes are proportional to $e^{2i\alpha_n}$. Assuming a uniform distribution of α in the interval $[-\Delta\alpha, +\Delta\alpha]$, we obtain

$$\begin{aligned} \langle V_n^2 \rangle - \langle V_n \rangle^2 &= V_0^2 [1 - \cos^4 \delta/2] \{ (\sin 2\Delta\alpha)/2\Delta\alpha \}^2 - \\ &\quad - (\sin 4\Delta\alpha)/4\Delta\alpha \approx (4/3) V_0^2 [1 - \cos^4 \delta/2] (\Delta\alpha)^{-2} \end{aligned}$$

for small $\Delta\alpha$. This yields

$$\ell_e \approx (3/V_0^2) \sin^2 |\mathbf{k}| (\Delta\alpha)^{-2} \cos^2(\delta/2) / [1 - \cos^4 \delta/2]. \quad (3)$$

Expression (3) shows that ℓ_e diverges as $\ell_e \sim (\Delta\alpha)^{-2} \delta^{-2}$ for small $\Delta\alpha$ and δ . Other more refined correspondences with the 1D tight-binding model recover this leading behavior. This simple reasoning is however insufficient to describe the dependence of the mean free path as a function of the Bloch wave directions of propagation.

We now describe the analytical calculation of the scattering of a Bloch wave of arbitrary wavevector \mathbf{k} and a single isolated defect, which will allow us to evaluate the elastic mean free time τ_e . In a periodic system, any propagating wave at a given pulsation ω can be described as a linear combination of Bloch waves $\mathbf{A}(\mathbf{k}, \tau)$ (with $\omega = \omega(\mathbf{k})$), the $4n^2$ components of each Bloch wave $\mathbf{A}(\mathbf{k}, \tau)$ being given by equations (16) and (26) of our previous paper [1a]. We introduce a perturbation in the medium, the S-matrix S_α is replaced, on one node (i, j) , by a different S-matrix $S_{\alpha'}$ (with $\alpha' \neq \alpha$). Any Bloch wave $\mathbf{A}(\mathbf{k}, \tau)$ encountering this defect at time τ , is scattered into a « scattered wave » : $\mathbf{B}(\mathbf{k}, \tau + 1)$. $\mathbf{B}(\mathbf{k}, \tau + 1)$ can be decomposed into a linear combination of Bloch waves of the unperturbed system :

$$\mathbf{B}(\mathbf{k}, \tau + 1) = \sum_{\mathbf{k}'(\omega = \omega(\mathbf{k}'))} |\langle \mathbf{A}(\mathbf{k}', \tau + 1) | \mathbf{B}(\mathbf{k}, \tau + 1) \rangle| \mathbf{A}(\mathbf{k}', \tau + 1) \quad (4)$$

$\mathbf{B}(\mathbf{k}, \tau + 1)$ is in fact almost equal to $\mathbf{A}(\mathbf{k}, \tau + 1)$, except for the fact that the four local fields impinging on the four neighboring nodes of node (i, j) are different from those deduced from the structure of $\mathbf{A}(\mathbf{k}, \tau + 1)$ due to the scattering process with the matrix $S_{\alpha'} \neq S_\alpha$. The complete expression of $\mathbf{B}(\mathbf{k}, \tau + 1)$ is given in appendix A. The fundamental hypothesis which allows us to consider $\mathbf{B}(\mathbf{k}, \tau + 1)$ as the scattered Bloch wave is the assumption of *single scattering*, i.e. that the wave interacts only once with the defect. This means that the four waves, which have been scattered off by the defect $S_{\alpha'}$ at node (i, j) , will never encounter again the defect $S_{\alpha'}$, but will only see the unperturbed S-matrix S_α on all nodes including (i, j) . This condition expresses the limit of single scattering taken in this computation.

Knowing the full expression of the scattered wave $\mathbf{B}(\mathbf{k}, \tau + 1)$, we are now in a position to derive the expression of the mean free time τ_e . The first step is to define the relative weight P of the scattering from the Bloch wave $\mathbf{A}(\mathbf{k}, \tau)$ to the Bloch wave $\mathbf{A}(\mathbf{k}', \tau + 1)$ at time $\tau + 1$, by the defect $S_{\alpha'}$ on node (i, j) . It is given by

$$P = \frac{|\langle \mathbf{A}(\mathbf{k}', \tau + 1) | \mathbf{B}(\mathbf{k}, \tau + 1) \rangle|^2}{\sum_{\mathbf{k}'(\omega = \omega(\mathbf{k}'))} |\langle \mathbf{A}(\mathbf{k}', \tau + 1) | \mathbf{B}(\mathbf{k}, \tau + 1) \rangle|^2} \quad (5)$$

The denominator allows us to normalize the weight to unity when summing over all outgoing Bloch waves, expressing the conservation of the energy.

We are interested in computing the so-called transport mean free time or mean free path, which will be of use in section 3 for calculating the transport properties of the wave in random media. In order to obtain the transport mean free time, we need to multiply the weight P for the scattering from channel \mathbf{k} to channel \mathbf{k}' by the factor $(1 - \cos \theta_{\mathbf{k}', \mathbf{k}}) = (1 - \mathbf{k} \cdot \mathbf{k}' / |\mathbf{k}| |\mathbf{k}'|)$, where $\theta_{\mathbf{k}', \mathbf{k}}$ is the angle between the two wavevectors \mathbf{k} and \mathbf{k}' .

$$P_{\mathbf{k}', \mathbf{k}} = P (1 - \cos \theta_{\mathbf{k}', \mathbf{k}}). \quad (6)$$

This factor puts a zero weight to the forward scattering and gives a maximum weight to the backward scattering. It takes into account the fact that the forward scattering does not correspond to a true scattering event [6].

To get the total fraction of the wave which has been scattered in all directions except the

incident one, we add all the contributions for the different outgoing channels \mathbf{k}' and obtain

$$P_{\mathbf{k}} = \sum_{\mathbf{k}'} P_{\mathbf{k}', \mathbf{k}}. \quad (7)$$

After one scattering event, the energy left in the \mathbf{k} direction is then $(1 - P_{\mathbf{k}})$.

Let us now consider an initially periodic medium in which all the sites are slightly modified to carry a matrix $S_{\alpha'} \neq S_{\alpha}$, with small random α' . In the limit where the perturbation created by the modification $\alpha' \neq 0$ is weak, we can use the superposition approximation over all the elementary scattering processes encountered by the initial Bloch wave. Then, the energy in the \mathbf{k} direction on the Bloch wave $\mathbf{A}(\mathbf{k}, \tau)$ after the time τ is decreased by the factor $(1 - P_{\mathbf{k}})^{\tau v_{\phi\mathbf{k}}} \approx \exp\{-P_{\mathbf{k}} v_{\phi\mathbf{k}} \tau\}$ in the limit of small $P_{\mathbf{k}}$, where $v_{\phi\mathbf{k}}$ is the phase velocity of the Bloch wave $\mathbf{A}(\mathbf{k})$. Indeed, the product $v_{\phi\mathbf{k}} \tau$ gives the number of sites encountered by the Bloch wave along a line of propagation in the direction \mathbf{k} , per unit length of the wave front. This allows us to define the transport mean free time $\tau_{\mathbf{k}}$ as :

$$\tau_{\mathbf{k}} = [v_{\phi\mathbf{k}} P_{\mathbf{k}}]^{-1} \quad (8)$$

$\tau_{\mathbf{k}}$ represents the characteristic decay time of the Bloch wave propagating along direction \mathbf{k} due to the presence of disorder. Note that equation (8) with (5) is nothing but the adaptation of the Fermi golden rule to the present problem.

The transport mean free time $\tau_c(\omega)$ of the disordered medium for a given pulsation ω is given by averaging the decay rate $1/\tau_{\mathbf{k}}$ over all the possible incident directions \mathbf{k} and over the disorder ($\alpha' \in [-\Delta\alpha, \Delta\alpha]$). This reads

$$\frac{1}{\tau_c(\omega)} = \left\langle \frac{1}{N_{\mathbf{k}}} \sum_{\mathbf{k}} \frac{1}{\tau_{\mathbf{k}}} \right\rangle_{\alpha' \in [-\Delta\alpha, \Delta\alpha]} \quad (9)$$

where $N_{\mathbf{k}}$ represents the total number of wavevectors \mathbf{k} which verify the dispersion relation $\omega(\mathbf{k}) = \omega$ for a fixed value of ω . The transport mean free time $\tau_c(\omega)$ is the average characteristic decay time of waves at frequency ω . It will be used in section 3. We do not present the general case of arbitrary pulsations ω but restrict our attention to the range of ω such that the dispersion relation is quadratic, and thus equivalent to a tight-binding or Schrödinger equation. This will allow us to use the prediction of weak localization calculations, which are available only in the case of quadratic dispersion relations [5]. In the parametrization in terms of α and δ in the wave automaton, pure quadratic dispersion relations exist only when the two branches given by equations (20a) and (20b) or (22a) and (22b) of reference [1a] can be separated. This occurs when a gap exists, i.e. for $\delta > \pi/2$. We also restrict our attention to values of ω close to and less than the band edge value $\omega^* = \pi - \delta$. This yields a number of domains for $\mathbf{k} = (k_x, k_y)$ over which the sum in equation (9) must be performed. These domains are defined in appendix B. Some important but tedious steps of the summation leading to the final expression of $\tau_c(\omega)$ are given in appendix C. The series of integrals must finally be performed numerically. In figure 1 is shown the result of these computations where $\tau_c(\omega)$ is drawn as a function of ω , in the neighborhood of the band edge where the calculation holds. The transport mean free path can then be obtained since it is just the product of $\tau_c(\omega)$ by the average wave velocity c at the pulsation ω . Note that the computation presented in figure 1 is valid only in the vicinity of the band edge.

3. Sub-diffusion and wave localization.

We now present our main numerical results obtained by implementing the wave automaton on a Connection Machine. Figure 2 shows a series of snapshots at different increasing times of the

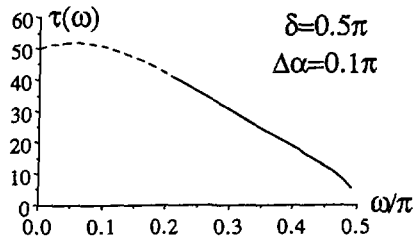


Fig. 1. — Dependence of the transport mean free time $\tau_e(\omega)$, obtained from the theory developed in the text, as a function of the pulsation ω for $\delta = 0.5 \pi$ and $\Delta\alpha = 0.1 \pi$. The analytical calculation is only valid near the band edge, $\omega = 0.5 \pi$.

wave intensity field within a random system with $\delta = \pi/2$ and $\Delta\alpha = 0.1 \pi$, after launching at the center of a system (the origin) of size 512 by 512 at $\tau = 0$ a narrow Gaussian wave packet of central pulsation $\omega = 0.47 \pi$ and width $\Delta\omega = 0.005 \pi$ (corresponding to a mean free path $\ell_e \approx 10$). For comparison figure 3 shows the same series of snapshots under the same conditions except that the wave, which is launched at the origin, consists in a Dirac impulse. In figure 2, a much smaller number of modes are excited whereas all modes in the system which overlap significantly with the origin are excited in figure 3. In figure 3, we clearly observe three regimes : the spreading of the wave packets is first ballistic for $\tau \leq 20$ less than the elastic mean free time ; for $20 \leq \tau \leq 80$, one can still observe the ballistic front whereas most of the wave energy has been scattered off and becomes diffusive. This ballistic-diffusive cross-over cannot be observed in the case of the wave packet (Fig. 2) because the source remains active over a time longer than the elastic mean free time. The analysis developed below will show that the diffusive regime is in fact subdiffusive. At much longer times of the order of 10^6 , the waves finally become localized. It is interesting to note the difference between the structures of the wave field at $\tau = 10^4$, represented in figures 2 and 3, for the Gaussian wave packet and for the Dirac impulse. The wave field is much more structured in the case of the Gaussian wave packet, due to the fact that a much smaller number of modes have been excited.

These observations are in qualitative agreement with the standard picture of wave transport in random media [8-10], according to which the wave is ballistic at scales longer than ℓ_e , diffusive at scales larger than ℓ_e , until one reaches the localization regime at scales larger than the localization length ξ . In order to exist, the third regime of Anderson localization needs a sufficiently strong disorder [8-10], in dimensions larger than two. The present understanding is that waves are always localized in two and less dimensions [8-10]. In practice however, the Anderson localization will be observed only when the system size is larger than the localization length ξ , which, in our systems, is a function of δ and $\Delta\alpha$.

Since figure 3 corresponds to a large superposition of excited modes, a kind of self-averaging occurs and only the global features of the transport are observed. This is particularly clear by taking the Fourier transform of the wave amplitude time dependence at the origin, as represented in figure 4a for the particular choice of parameters $\delta = 0.9 \pi$ and $\Delta\alpha = 0.2 \pi$. This choice of parameters entails a very short localization length of the order of a few lattice meshes. Therefore, the Dirac impulse excites all modes whose locations are within a localization length of the origin. Because they are relatively few, well-defined peaks corresponding to the eigenfrequencies can be observed. Note that the Fourier transform of the same signal as for the Dirac impulse shown in figure 3 would give such a dense system of peaks that they would form a very dense system of peaks on this scale $-0.25 \leq f \leq 0.25$ due to the much larger number of modes which are excited in this case. Figure 4b presents the Fourier transform of the time evolution of a Dirac impulse propagation on a periodic system

with $\delta = 0.9 \pi$ and $\Delta\alpha = 0$. The eigenfrequencies form a dense set in the interval $-0.05 \leq f \leq 0.05$ (as expected the passing band width is 0.1π (see [1a]). Note that the effect of disorder is to populate the stop bands of the periodic system. Very sharp peaks can be observed centered on the eigenfrequencies of the random system. We note that the density of peaks defines a nearly constant average density of states (the average spacing between neighboring peaks seems to be independent of the frequency). This was expected since the

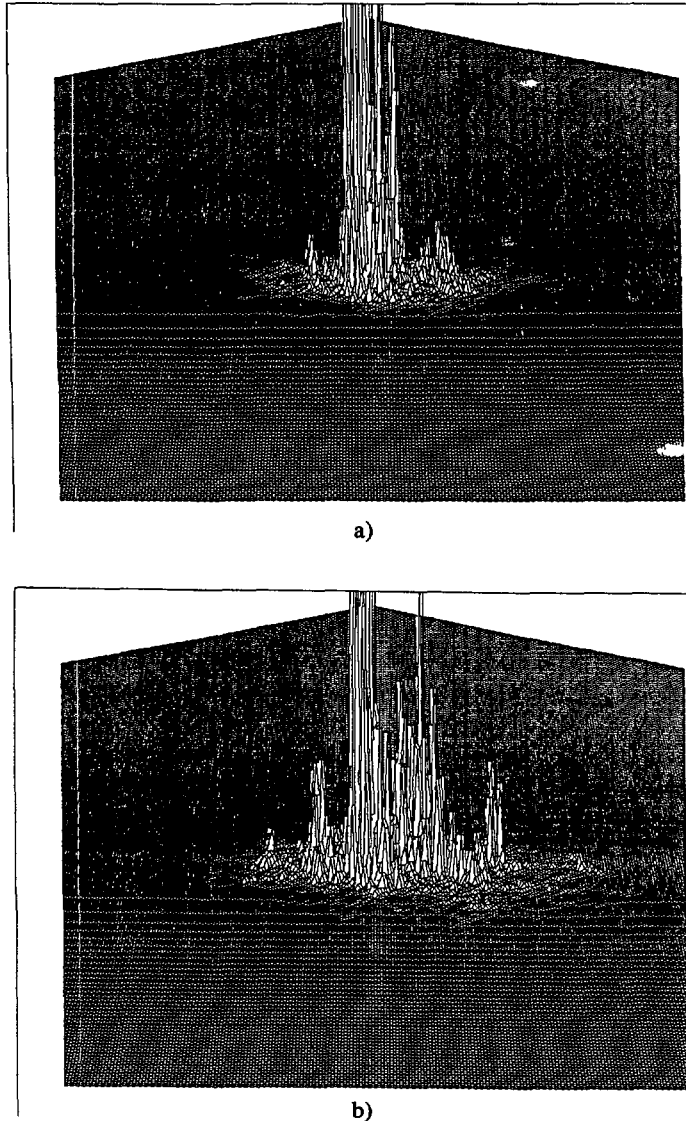


Fig. 2. — Series of snapshots at different increasing times of the wave intensity field within a random system with $\delta = \pi/2$ and $\Delta\alpha = 0.1 \pi$, after launching at the center of a system (the origin) of size 512 by 512 at $\tau = 0$ a narrow Gaussian wave packet of central pulsation $\omega = 0.47 \pi$ and width $\Delta\omega = 0.005 \pi$. Figures a to d are closeups which show only a small central part of the system. The figure shows the entire lattice. a) $\tau = 500$; b) $\tau = 1\ 000$; c) $\tau = 10\ 000$; d) $\tau = 10\ 000$ showing the entire lattice. Note that the lattice in figure 2d has nothing to do with the original lattice but is drawn for the purpose of representation.

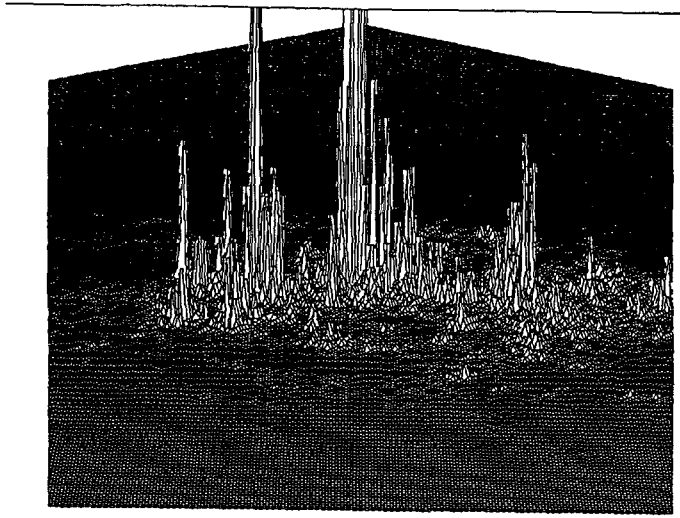


Fig. 2c.

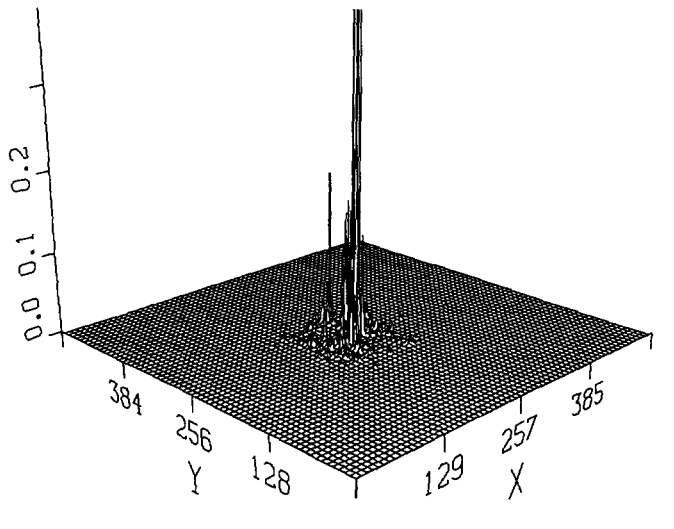


Fig. 2d.

density of states in the periodic case is already constant for $\delta \leq \omega \leq \pi/2$ and does not vary significantly except near $\omega = 0$, as seen in figure 8 of reference [1a]. We have verified that the distribution of spacings $\delta\omega$ between consecutive eigenpulsations is Poissonian, in agreement with the general theory of random matrices [11]. This result is well-known in 1D random systems and is characteristic of localized modes [12]. It is thus interesting to confirm that the Poissonian distribution seems robust in higher dimensions. Physically, the Poissonian nature of the distribution of level spacings stems from the superposition of many quasi-independent sub-systems of size of the order of the localization length.

In contrast, a much smaller number of modes are excited in the case of figure 2 and the complexity of the observed intensity field thus reflects that of the eigenmodes. To illustrate this

point further, figure 5 shows the wave intensity field of a pure eigenmode at frequency $f = 0.228714$ in the case $\delta = 0.5 \pi$ and $\Delta\alpha = 0.3 \pi$, obtained by using a source placed at the origin which oscillates at the pulsation frequency $f = 0.228714$, and whose amplitude has been increased from zero very slowly over a long timespan $\Delta\tau \approx 10^5$ in order to minimize the number ($< 10^{-5} L^2 \approx 10$) of excited modes in the frequency range $\Delta f \approx 10^{-5}$ around the

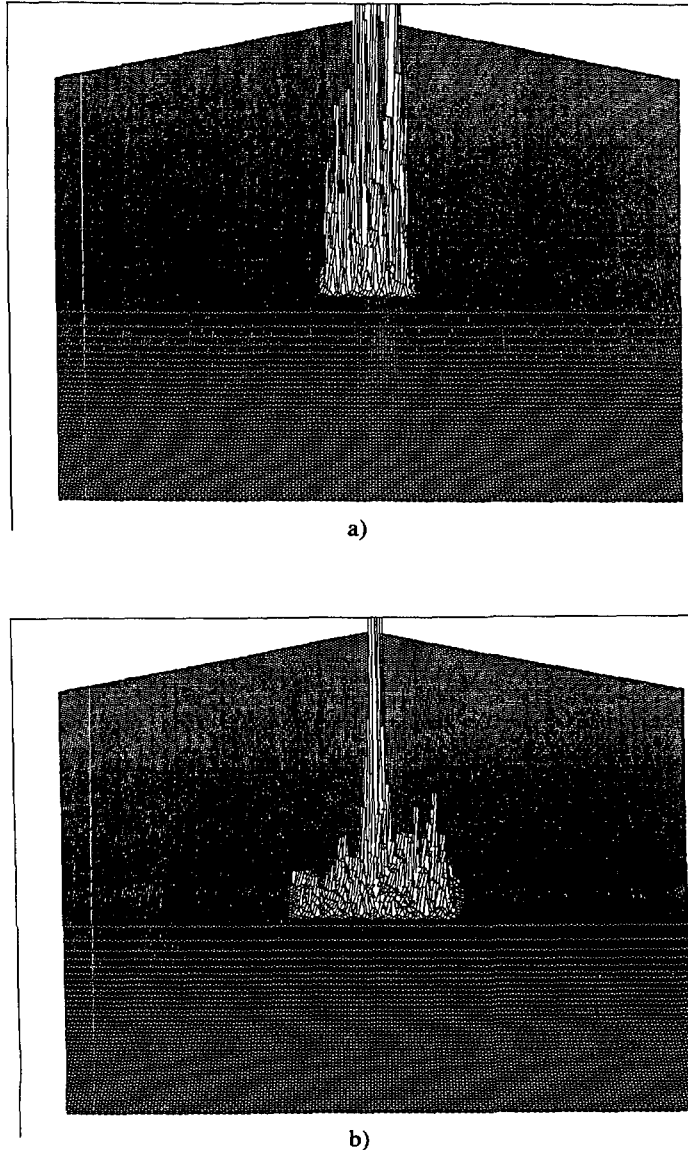


Fig. 3. — Same as in figure 2 except that the wave, which is launched at the origin, consists in a Dirac impulse. Figures a to f are closeups which show only a small central part of the system. a) $\tau = 20$; b) $\tau = 40$; c) $\tau = 60$; d) $\tau = 80$; e) $\tau = 100$; f) $\tau = 200$; g) $\tau = 10\,000$ for the entire lattice. The vertical scale has been enhanced by a factor 10 in figure g). Note that the lattice shown in figure 3g has nothing to do with the original lattice but is drawn for the purpose of representation.

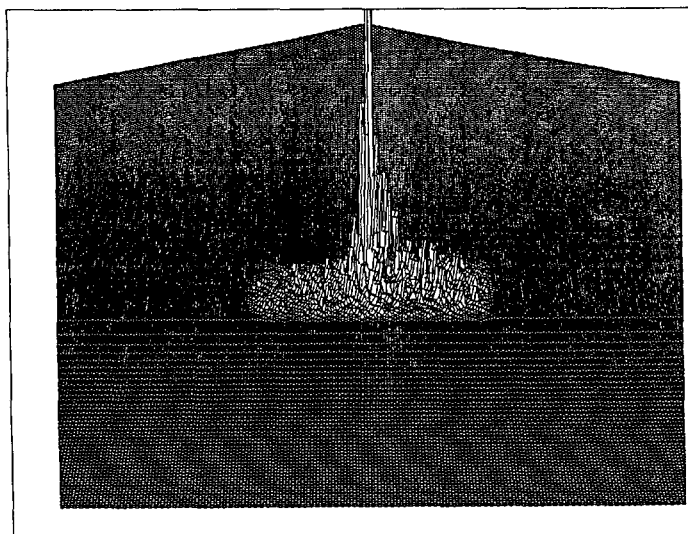


Fig. 3c.

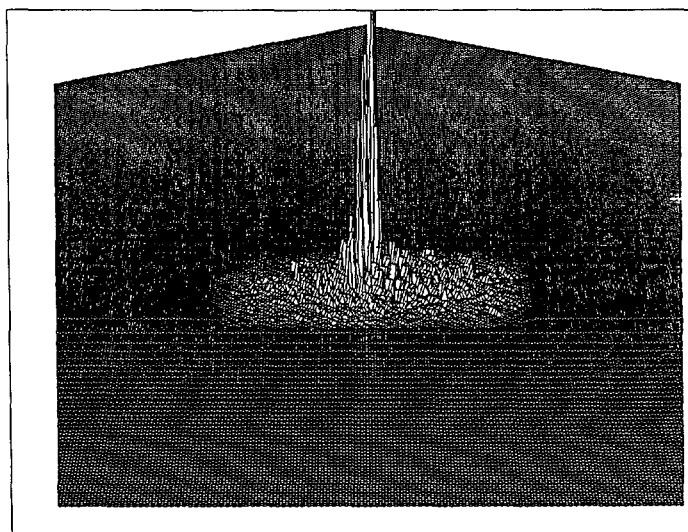


Fig. 3d.

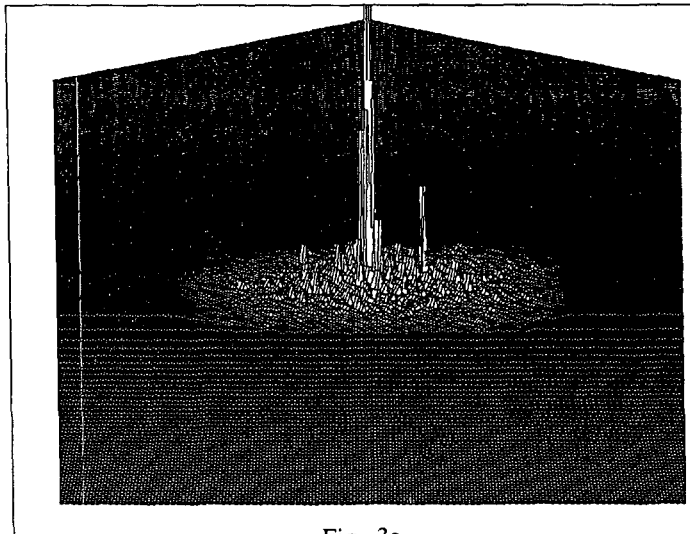


Fig. 3e.

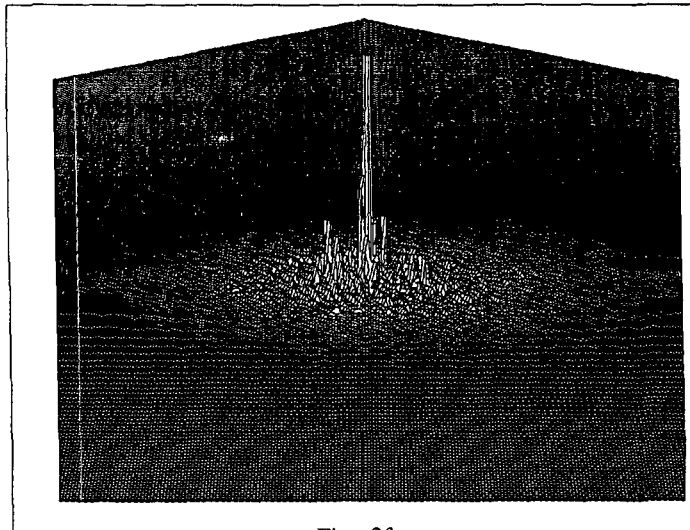


Fig. 3f.

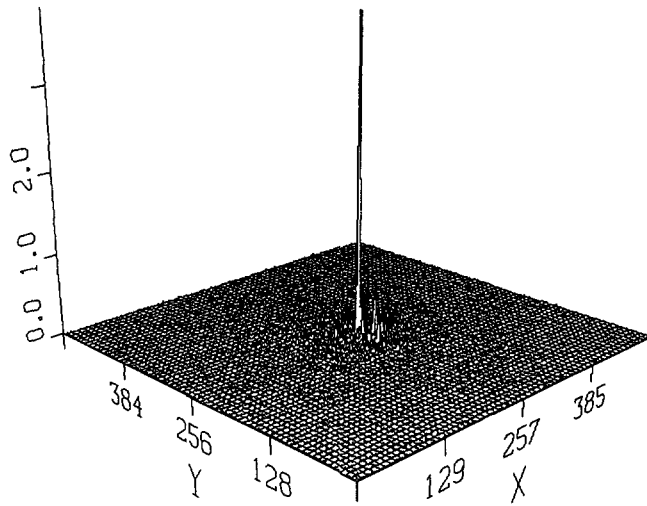
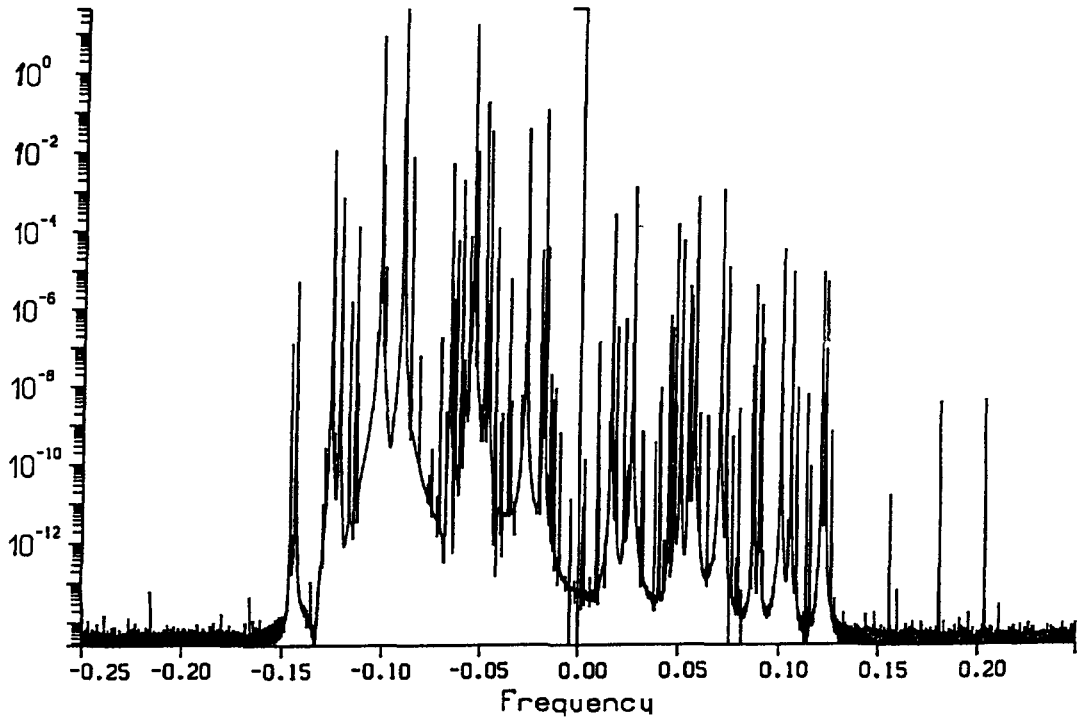


Fig. 3g.



a)

Fig. 4. — a) Fourier transform of the wave amplitude time dependence at the origin as a function of the frequency f in the case $\delta = 0.9 \pi$ and $\Delta\alpha = 0.2 \pi$. b) Same as a) but in the corresponding periodic lattice $\delta = 0.9 \pi$ and $\Delta\alpha = 0$.

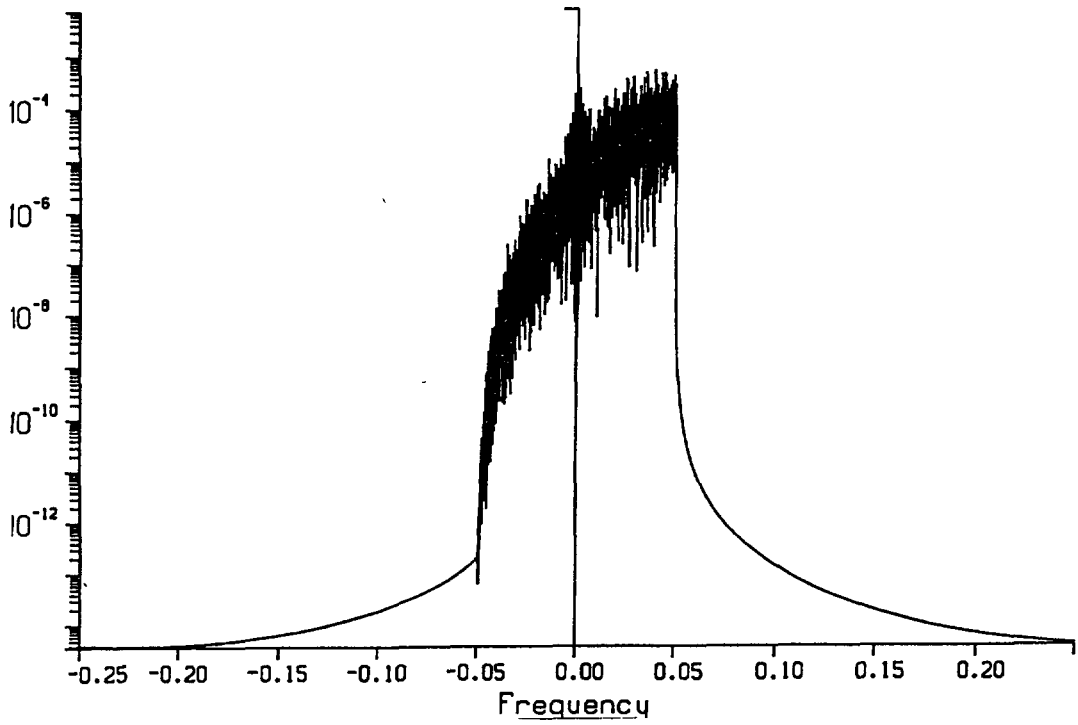


Fig. 4b.

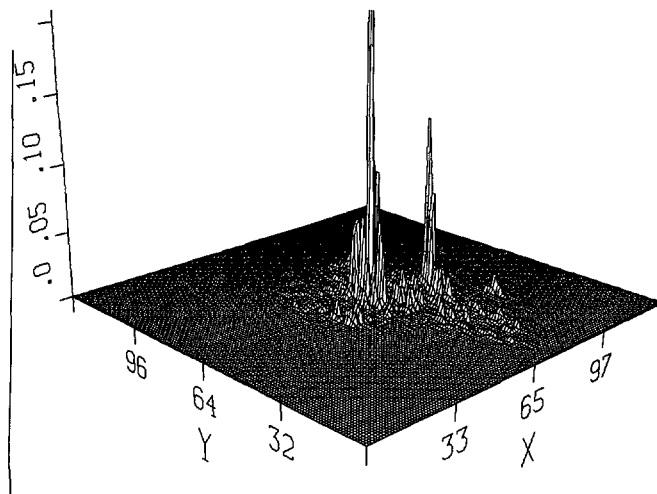


Fig. 5. — Wave intensity field of a pure eigenmode of frequency $f = 0.228714$ in a random system with $\delta = 0.5 \pi$ and $\Delta\alpha = 0.3 \pi$.

frequency $f = 0.228714$. Then, keeping the source functioning over a long time $\approx 10^6$ at a constant amplitude allows us to amplify the mode linearly in time by resonance at $f = 0.228714$, whereas all the other modes which may have been excited have their amplitude remain constant. We check that the obtained wave field corresponds to the single mode at $f = 0.228714$, by Fourier transforming the wave amplitude time dependence at the origin after the source has been finally cut down. One indeed observes the existence of a single peak of intensity $> 10^5$ above all others. More directly, we verify that all points of the lattice oscillate with the same frequency f . Although we have not carried out a specific study of the spatial properties of the eigenmodes, the spatially intermittent structure of the eigenmodes with the presence of quite many different scales is in qualitative agreement with previous studies [13] which have shown that the localized eigenmodes are fractal and may be even multifractal up the cut-off length imposed by the finite localization length ξ .

Figure 6 shows the radius of gyration or mean square width $|R^2|^{1/2} = |\langle \Psi(\mathbf{r}) | |\mathbf{r}|^2 | \Psi(\mathbf{r}) \rangle|^{1/2}$ of the spreading wave packet as a function of time up to $\tau = 10^6$ launched from an initial Diract impulse at the origin, for $\delta = 0.83 \pi$ and $\Delta\alpha = 0.1 \pi$ for two boundary conditions : periodic (upper curve) and open (lower curve). Note that the two curves are indistinguishable except at the largest times at which the tails of the wave packet reach the system border. Here, $|R^2|^{1/2}$ is not averaged over different realizations of the disorder but corresponds to a single specific realization. The observed self-averaging stems from the superposition of the hundred of thousands modes which are excited in this configuration and which overlap on the frequency axis for times less than the inverse average spacing between eigenfrequencies. At longer times, beating becomes significant. For systems with larger disorders so that the number of modes in a localization volume is largely decreased, we also observe significant fluctuations of $|R^2|^{1/2}$ as a function of time.

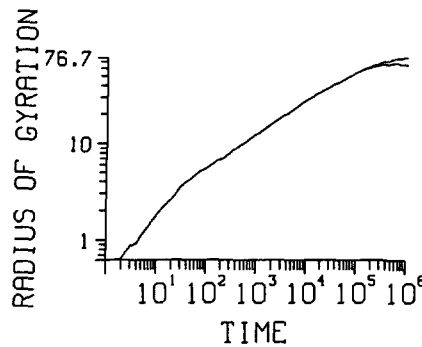


Fig. 6. — Radius of gyration $|R^2|^{1/2} = |\langle \Psi(\mathbf{r}) | |\mathbf{r}|^2 | \Psi(\mathbf{r}) \rangle|^{1/2}$ as a function of time up to $\tau = 10^6$ (the inverse bandwidth corresponds to $\tau = 2$) for $\delta = 0.83 \pi$ and $\Delta\alpha = 0.1 \pi$ for two boundary conditions : periodic (upper curve) and open (lower curve).

Instead of the usual diffusive behavior expected at scales $\ell_c \ll |\mathbf{r}| \ll \xi$, we observe a sub-diffusive dynamics in which the mean square width $|R^2|$ of an initial narrow pulse launched at $\tau = 0$ scales as $|R^2| \sim \tau^{2\nu}$, with an exponent $\nu = 0.45$ significantly less than $1/2$ and varying continuously as a function of the disorder. This observation of a sub-diffuse regime, with an exponent $\nu \ll 1/2$, allows to us refine the standard picture of localization according to which a wave packet diffuses at short times before realizing it is trapped as in an effective cavity of size given by the localization length. The observation of such a diffusive regime has previously

been announced in numerical studies in [14] and predicted on the basis of weak localization calculations in [5]. In order to understand better this subdiffusive regime, in figure 7 we report the dependence of $|R^2|^{1/2}$ as a function of time for different values of the scattering strength (same $\Delta\alpha = 0.4 \pi$ and increasing δ by 0.1π units from 0.1π to 0.8π from top to bottom). All curves are characterized by three regimes, 1) ballistic at very short times for $|R^2|^{1/2} < \ell_e$, 2) sub-diffusive at intermediate times for $\ell_e \leq |R^2|^{1/2} \leq \xi$ and 3) localized at long times. For the smallest δ , the localized regime is not observed since the localization length is larger than the system size. For the largest δ , the subdiffusive regime disappears since localization occurs at the scale of the lattice mesh. The dependence of ν as a function of δ is shown in figure. The exponent ν decreases from its classical diffusive value $1/2$ as the scattering strength increases.

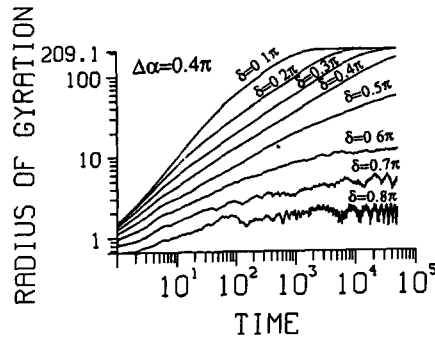


Fig. 7. — Dependence of $|R^2|^{1/2}$ as a function of time for different values of the scattering strength (same $\Delta\alpha = 0.4 \pi$ and increasing δ by 0.1π units from 0.1π to 0.8π from top to bottom).

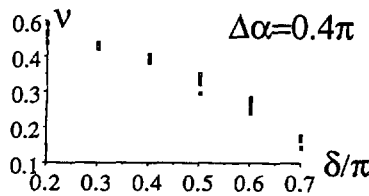


Fig. 8. — Dependence of ν as a function of δ ($\Delta\alpha$ being kept fixed) in the case where a Dirac impulse is launched at the origin (case represented in Fig. 7).

This subdiffusion stems from weak localization effects. Indeed, consider the weak localization formula for the diffusion coefficient at large scale L of a wave packet centered on ω : $D(L) = D_0[1 - (2 \omega \tau_e)^{-1} \text{Log} (L/\ell_e)]$, where $\tau_e(\omega)$ is the characteristic decay time calculated in equation (9). Taking $\tau/\tau_e \sim (L/\ell_e)^2$, this yields $D(\tau) = D_0[1 - (\omega \tau_e)^{-1} \text{Log} (\tau/\tau_e)]$. Using $|R^2| = 4 D(\tau) \tau$, we recover precisely the time dependent weak localization perturbation calculations [5]. Using the fact that to first order, $1 - (\omega \tau_e)^{-1} \text{Log} (\tau/\tau_e) \approx (\tau/\tau_e)^{-1/\omega \tau_e}$, we thus obtain

$$\nu = 1/2 - (2 \omega \tau_e)^{-1} \tag{10}$$

Equation (10) explains qualitatively the result of figure 8 that ν decreases as τ_e or ℓ_e decreases. However, no precise quantitative analysis is possible with a Dirac pulse since it does not fulfill the conditions for the weak localization calculations to be valid. Indeed, equation (10) holds only for narrow wave packets of central pulsation ω and width $\Delta\omega \ll \omega$. In order to test quantitatively the time dependent weak localization calculations [5], we now consider the simulations of the spreading of wave packets using a set of parameters such that all the conditions required for the weak localization expression (10) to hold are satisfied. The central pulsation ω is chosen close to a gap (which exists for $\delta \geq \pi/2$ so that the dispersion relation $\omega(\mathbf{k})$ is quadratic), thereby ensuring that our wave automaton model is quantitatively equivalent to a short-range tight-binding model. Figure 9 presents the dependence of ν as a function of ω for $\delta = \pi/2$ and $\Delta\alpha = 0.1 \pi$. This set of parameters constitutes the best trade off for quantifying with precision the subdiffusive behavior (a disorder which is not too weak to observe the effect and not too strong so that subdiffusion still exists). Note also that when ω approaches the band edge ($\omega = 0.5 \pi$ in this case), the localization length becomes very small and the subdiffusive regime is hardly observable. On the contrary, when ω is far from $\pi/2$, the correction to the classical value $\nu = 1/2$ becomes small and the dispersion relation begins to deviate significantly from being quadratic. We find large fluctuations (in the ratio of one to several thousands) from realization to realization in the amount of energy coupled inside the system, which can be attributed to local resonances at ω of the transient source with localized proper modes placed near the origin. This means that the diffusion of the wave packet is controlled by a wildly fluctuating number of excited modes. As a consequence, we have found ensemble averaging unreliable since the results do not seem to improve significantly as the number of realizations is increased (say from 10 to 100). The points obtained numerically which are shown in figure 9 have been obtained by taking the most probable value of the slope of $\text{Log } |R^2|$ as a function of $\text{Log } \tau$. The bars give our estimate of the fluctuations around this most probable value. The theoretical expression [5] (Eq. (10)) is given by the crosses for comparison. We find a good quantitative agreement, with however a systematic deviation as ω approaches the band edge, which is not surprising since the first order perturbation theory becomes unreliable as the perturbative parameter $1/\omega \tau_e$ becomes larger.

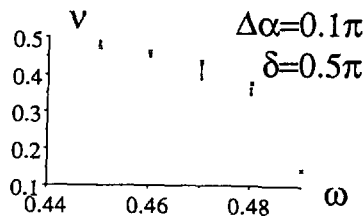


Fig. 9. — Dependence of the exponent ν as a function of ω for $\delta = \pi/2$ and $\Delta\alpha = 0.1 \pi$, in the case where a Gaussian wave packet of central pulsation ω chosen close to a gap and of width $\Delta\omega = 0.005 \pi$ is launched at the origin. The numerical results are represented by the vertical bars and the theoretical predictions (see text) correspond to the crosses.

4. Conclusion.

We have analyzed quantitatively the time evolution of the spreading of a wave packet in a 2D disordered system. The observed subdiffusive regime has been explained quantitatively in terms of a time dependent weak localization correction to the diffusion coefficient. The good

agreement between weak localization theory and our numerical computations has been made possible by using a direct determination of the elastic mean free time, which quantifies the scattering efficiency of Bloch waves by S-matrix scatterers.

Acknowledgments.

We are grateful to J.-P. Bouchaud and S. Feng for stimulating discussions, R. Fournier for introducing us to computing on CM2 and D. Stauffer for his constructive remarks. This work was partially supported by DRET under contract 89/271. The computations have been carried out on the Connection Machine of INRIA in Sophia Antipolis and of Institut de Physique du Globe in Paris.

Appendix A.

Expression of the wave $\mathbf{B}(\mathbf{k}, \tau + 1)$ scattered by a scatterer on node (i_0, j_0) in terms of Bloch waves $\mathbf{A}(\mathbf{k}, \tau + 1)$:

$$\begin{aligned}
 \text{on node } (i_0, j_0 + 1): \mathbf{B}_{\mathbf{k}}^{(i_0, j_0 + 1)}(\tau + 1) &= \begin{bmatrix} e^{-2i(\alpha - \alpha')} \mathbf{A}_1^{(i_0, j_0 + 1)}(\tau + 1) \\ \mathbf{A}_2^{(i_0, j_0 + 1)}(\tau + 1) \\ \mathbf{A}_3^{(i_0, j_0 + 1)}(\tau + 1) \\ \mathbf{A}_4^{(i_0, j_0 + 1)}(\tau + 1) \end{bmatrix} \\
 \text{on node } (i_0, j_0 - 1): \mathbf{B}_{\mathbf{k}}^{(i_0, j_0 - 1)}(\tau + 1) &= \begin{bmatrix} \mathbf{A}_1^{(i_0, j_0 - 1)}(\tau + 1) \\ e^{2i(\alpha - \alpha')} \mathbf{A}_2^{(i_0, j_0 - 1)}(\tau + 1) \\ \mathbf{A}_3^{(i_0, j_0 - 1)}(\tau + 1) \\ \mathbf{A}_4^{(i_0, j_0 - 1)}(\tau + 1) \end{bmatrix} \\
 \text{on node } (i_0 + 1, j_0): \mathbf{B}_{\mathbf{k}}^{(i_0 + 1, j_0)}(\tau + 1) &= \begin{bmatrix} \mathbf{A}_1^{(i_0 + 1, j_0)}(\tau + 1) \\ \mathbf{A}_2^{(i_0 + 1, j_0)}(\tau + 1) \\ e^{-2i(\alpha - \alpha')} \mathbf{A}_3^{(i_0 + 1, j_0)}(\tau + 1) \\ \mathbf{A}_4^{(i_0 + 1, j_0)}(\tau + 1) \end{bmatrix} \\
 \text{on node } (i_0 - 1, j_0): \mathbf{B}_{\mathbf{k}}^{(i_0 - 1, j_0)}(\tau + 1) &= \begin{bmatrix} \mathbf{A}_1^{(i_0 - 1, j_0)}(\tau + 1) \\ \mathbf{A}_2^{(i_0 - 1, j_0)}(\tau + 1) \\ \mathbf{A}_3^{(i_0 - 1, j_0)}(\tau + 1) \\ e^{2i(\alpha - \alpha')} \mathbf{A}_4^{(i_0 - 1, j_0)}(\tau + 1) \end{bmatrix}.
 \end{aligned}$$

For all other nodes $(i, j): \mathbf{B}_{\mathbf{k}}^{(i, j)}(\tau + 1) = \mathbf{A}_{\mathbf{k}}^{(i, j)}(\tau + 1)$.

We deduce $|\langle \mathbf{A}_{\mathbf{k}'} | \mathbf{B}_{\mathbf{k}} \rangle|^2$ using expressions (26) of [1] giving the Bloch wave coefficients. We thus obtain

$$|\langle \mathbf{A}_{\mathbf{k}'} | \mathbf{B}_{\mathbf{k}} \rangle|^2 = |e^{2i(\alpha - \alpha')}|^2 \frac{U^2 + V^2}{DD'}$$

with

$$U = \cos(k'_v - k_v)/2 [\cos(k'_v - k_v)/2 - \cos \omega \cos(k'_v + k_v)/2] XX' + \\ + \cos(k'_\lambda - k_\lambda)/2 [\cos(k'_\lambda - k_\lambda)/2 - \cos \omega \cos(k'_\lambda + k_\lambda)/2] YY'$$

$$V = 1/2 \sin \omega (\cos k'_v - \cos k_v) XX' + 1/2 \sin \omega (\cos k'_\lambda - \cos k_\lambda) YY'$$

$$D = (1 - \cos \omega \cos k_v) X^2 + (1 - \cos \omega \cos k_\lambda) Y^2$$

$$D' = (1 - \cos \omega \cos k'_v) X'^2 + (1 - \cos \omega \cos k'_\lambda) Y'^2$$

where

$$X = \cos(\omega - \delta/2) - \cos k_v \cos \delta/2 \quad X' = \cos(\omega - \delta/2) - \cos k'_v \cos \delta/2$$

$$Y = \cos(\omega - \delta/2) - \cos k_\lambda \cos \delta/2 \quad Y' = \cos(\omega - \delta/2) - \cos k'_\lambda \cos \delta/2.$$

Appendix B.

Domains of integration for the calculation of the mean free path defined by $\omega(\mathbf{k}) = \omega$: equations (20b) and (22b) of reference [1a] give

$$-2 \sqrt{(\omega^* - \omega) \operatorname{tg} \delta/2} < k'_\lambda < +2 \sqrt{(\omega^* - \omega) \operatorname{tg} \delta/2} \quad (\text{domaine } d_1)$$

and

$$k'_v = h_1(\omega, k_\lambda) = \sqrt{4(\omega^* - \omega) \operatorname{tg} \delta/2 - k'_\lambda{}^2}$$

or

$$k'_v = h_2(\omega, k_\lambda) = -\sqrt{4(\omega^* - \omega) \operatorname{tg} \delta/2 - k'_\lambda{}^2}$$

where ω^* is the frequency of the band edge.

Equation (23a) of reference [1a] gives

$$\pi - 2 \sqrt{(\omega^* - \omega) \operatorname{tg} \delta/2} < k'_\lambda < \pi \quad (\text{domaine } d_2)$$

and

$$k'_v = h_3(\omega, k_\lambda) = [\pi - \sqrt{4(\omega^* - \omega) \operatorname{tg} \delta/2 - (\pi - k'_\lambda)^2}]$$

or

$$k'_v = h_4(\omega, k_\lambda) = -[\pi - \sqrt{4(\omega^* - \omega) \operatorname{tg} \delta/2 - (\pi - k'_\lambda)^2}]$$

$$-\pi < k'_\lambda < -\pi + 2 \sqrt{(\omega^* - \omega) \operatorname{tg} \delta/2} \quad (\text{domaine } d_3)$$

and

$$k'_v = h_5(\omega, k_\lambda) = [\pi - \sqrt{4(\omega^* - \omega) \operatorname{tg} \delta/2 - (\pi + k'_\lambda)^2}]$$

or

$$k'_v = h_6(\omega, k_\lambda) = -[\pi - \sqrt{4(\omega^* - \omega) \operatorname{tg} \delta/2 - (\pi + k'_\lambda)^2}].$$

The sum over wavevectors in the determination of the transport mean free time must thus be performed over these three domains.

Appendix C.

Final expression of the free mean time $\tau_e(\omega)$:

— the average over the disorder, when $\alpha = 0$, gives the contribution :

$$\langle |e^{-2i\alpha} - 1|^2 \rangle_{\alpha \in [-\Delta\alpha, \Delta\alpha]} = 2 \left(1 - \frac{\sin 2\Delta\alpha}{2\Delta\alpha} \right)$$

— the discrete sum of any function $f(\mathbf{k})$ over the \mathbf{k} 's becomes :

$$\begin{aligned} \sum_{\mathbf{k} \text{ such } \omega(\mathbf{k}) = \omega} f(\mathbf{k}) &= \sum_{\mathbf{k}} \delta_{\omega, \omega(\mathbf{k})} f(\mathbf{k}) = \sum_{k_x, k_y} \delta_{\omega, \omega(k_x, k_y)} f(k_x, k_y) = \\ &= \sum_{k_x, k_y} \delta_{k_x, h_j(\omega, k_x)} f(k_x, k_y) \\ &= \int_{d_i} \frac{dk_x}{2\pi/L} \int dk_y \delta(k_x - h_j(\omega, k_x)) f(k_x, k_y) = \int_{d_i} \frac{dk_x}{2\pi/L} f(k_x, h_j(\omega, k_x)) \end{aligned}$$

where d_i and h_j are respectively one of the three domains of k_x and one of the six expressions of k_y given in appendix B ;

— we also have

$$\cos \theta_{\mathbf{k}', \mathbf{k}} = \frac{k_x k'_x + k_y k'_y}{\sqrt{k_x^2 + k_y^2} \sqrt{k_x'^2 + k_y'^2}}$$

and

$$N_{\mathbf{k}} = \frac{8L}{2\pi} \sqrt{(\omega^* - \omega) \operatorname{tg} \delta/2}.$$

The final expression for $\tau_e(\omega)$ is given by

$$\frac{1}{\tau_e(\omega)} = \frac{\left[1 - \frac{\sin 2\Delta\alpha}{2\Delta\alpha} \right]}{4(\omega^* - \omega) \operatorname{tg} \delta/2} Q$$

where

$$\begin{aligned} Q &= \int_{d_1} dk_x F(k_x, h_1(\omega, k_x)) + \int_{d_1} dk_x F(k_x, h_2(\omega, k_x)) + \int_{d_2} dk_x F(k_x, h_3(\omega, k_x)) + \\ &+ \int_{d_2} dk_x F(k_x, h_4(\omega, k_x)) + \int_{d_3} dk_x F(k_x, h_5(\omega, k_x)) + \int_{d_3} dk_x F(k_x, h_6(\omega, k_x)) \end{aligned}$$

where $F(k_x, h_j(\omega, k_x)) =$

$$\begin{aligned} &\frac{\int_{d'_1} dk'_x [G(k'_x, h_1(\omega, k'_x)) + G(k'_x, h_2(\omega, k'_x))] + \int_{d'_2} dk'_x [G(k'_x, h_3(\omega, k'_x)) + G(k'_x, h_4(\omega, k'_x))] \dots}{\int_{d'_1} dk'_x [K(k'_x, h_1(\omega, k'_x)) + K(k'_x, h_2(\omega, k'_x))] + \int_{d'_2} dk'_x [K(k'_x, h_3(\omega, k'_x)) + K(k'_x, h_4(\omega, k'_x))] \dots} \\ &+ \frac{\int_{d'_3} dk'_x [G(k'_x, h_5(\omega, k'_x)) + G(k'_x, h_6(\omega, k'_x))] \dots}{\int_{d'_3} dk'_x [K(k'_x, h_5(\omega, k'_x)) + K(k'_x, h_6(\omega, k'_x))] \dots} \end{aligned}$$

and where $G(k'_x, h_j(\omega, k'_x)) = \frac{U^2 + V^2}{DD'} [1 - \cos \theta_{\mathbf{k}', \mathbf{k}}]$

and

$$K(k'_i, h_j(\omega, k'_i)) = \frac{U^2 + V^2}{DD'}$$

The expressions for U , V , D and D' are given in appendix A.

References

- [1] a) SEBBAH P., SORNETTE D. and VANNESTE C., A wave automaton for wave propagation in the time domain : I-Periodic systems, *J. Phys. I France* **3** (1993) ;
 b) VANNESTE C., SEBBAH P. and SORNETTE D., *Europhys. Lett.* **17** (1992) 715-720 ; **18** (1992) 567 (Erratum).
- [2] KOONIN S. E., Computational Physics (Benjamin/Cummins, Menlo Park, Cal., 1986).
- [3] SMITH G. D., Numerical solution of Partial Differential Equations : Finite Difference Methods (Clarendon Press, Oxford, 1985).
- [4] DE RAEDT H., *Europhys. Lett.* **3** (1987) 139 ; *Comp. Phys. Rep.* **7** (1987) 1 ;
 HUYGHEBAERT J. and DE RAEDT H., *J. Phys. A : Math. Gen.* **23** (1990) 5777.
- [5] NAKHMEDOV E. P. and PRIGODIN V. N. and FIRTOV Yu. A., *Sov. Phys. JEPT* **65** (1987) 1202.
- [6] ISHIMARU A., Wave propagation and scattering in random media (Academic Press, New York, N.Y., 1978).
- [7] ISHII K., *Suppl. Progr. Theor. Phys.* **53** (1973) 7 ;
 ZIMAN J. M., Models of disorder (Cambridge University Press, Cambridge, 1979).
- [8] LEE P. A. and RAMAKRISHNAN T. V., *Rev. Mod. Phys.* **57** (1985) 287.
- [9] SOUILLARD B., Waves and electrons in inhomogeneous media, in Les Houches, Session XLVI, 1986, Chance and Matter, J. Souletie, J. Vannimenus and R. Stora Eds. (North Holland, Amsterdam, 1987).
- [10] SORNETTE D., *Acustica* **67** (1989) 199 ; **67** (1989) 251 ; **68** (1989) 15.
- [11] MEHTA M. L., RANDOM Matrices and the Statistical Theory of Energy Levels (Academic Press, New York, 1967) p. 14.
- [12] POKROVSKII V. L., *ZhETF Pis ma* **4** (1966) 140-144 ;
 MOLCANOV S. A., *Commun. Math. Phys.* **78** (1981) 429 ;
 FEINGOLD M. and FISHMAN S., *Physica* **25D** (1987) 181 ;
 IZRAILEV F. M., *J. Phys. A : Math. Gen.* **22** (1989) 865.
- [13] a) PICHARD J. L. and SARMA G., Powerlaw decay and fractal character of eigenstates in two-dimensional disordered systems, *J. Phys. C* **18** (1985) 3457 ;
 b) SCHREIBER M., Numerical characterization of electronic states in disordered systems. Inst. Phys. Conf. Ser. N° 108, Paper presented at the Localization 1990 Conference held at Imperial College, London, 13-15 August 1990, p. 65-76 (1991 IOP Publishing Ltd) ; Fractal eigenstates in disordered systems, *Physica A* **167** (1990) 188 ;
 c) AOKI H., Critical behaviour of extended states in disordered systems, *J. Phys. C* **16** (1983) L205 ;
 d) CASTELLANI C. and PELITI L., *J. Phys. A* **19** (1986) L492 ; **19** (1986) L1099 ;
 e) AOKI H., Fractal dimensionality of wave functions at the mobility edge : Quantum fractal in the Landau levels, *Phys. Rev. B* **33** (1986) 7310 ;
 f) POOK W. and JANBEN M., Multifractality and scaling in disordered mesoscopic systems, *Z. Phys. B* **82** (1991) 295 ;
 g) SCHREIBER M. and GRUSSBACH H., *Phys. Rev. Lett.* **67** (1991) 607 ;
 h) DE VRIES P., DE RAEDT H. and LAGENDIJK A., Localization of waves in Fractals : Spatial behavior, *Phys. Rev. Lett.* **62** (1989) 2515 ;

- i) EVANGELOU S. N., Scaling exponents at the mobility edge, *Physica A* **167** (1990) 199.
 - j) CHALKER J. T., Scaling and eigenfunction correlations near the mobility edge, *Physica A* **167** (1990) 253.
- [14] SCHER G. M., *J. Non-Cryst. Solids* **69** (1983) 33 ;
KAVEH M., *Philos. Mag. B* **52** (1985) 521 ;
HAYDOCK R., *Philos. Mag. B* **53** (1986) 545-559.